Multibody System Dynamics **7:** 389–406, 2002.

Dynamic Modeling of the Human Arm with Video-Based Experimental Analysis

ETTORE PENNESTRÌ, ADRIANO RENZI and PAOLO SANTONOCITO
Dipartimento di Ingeneria Meccanica, Università degli Studi di Roma 'Tor Vergata', via di Tor Vergata 110, I-00133 Roma, Italy

(Received: 22 February 2000; accepted in revised form: 27 July 2000)

Abstract. The quantitative assessment of human joint torque capability has many important applications. By means of a multibody approach, the authors described a formulation for 3D inverse dynamic analysis of a human arm during voluntary free movement. In particular, it is presented as a test case where the kinematics of the arm is obtained by means of a video-based human motion analysis system.

Key words: inverse dynamics, biodynamic modeling, human motion analysis.

Nomenclature

$[A_i] = [E_i][G_i^T]$	= transformation matrix of the ith body
C_i	= center of mass of the ith body
$\{e_i\}$	= the set of Euler parameters of the ith body
$\{F_w\}$	= generalized forces due to weight
$\{F_c\}$	= generalized forces due to centrifugal terms
$[J_i]$	= inertia matrix of the ith body
$\{Q\}$	= external generalized forces
$\{T_{ij}\}^{(i)} = \{T_{ij_{x_i}}\ T_{ij_{y_i}}\ T_{ij_{z_i}}\}^T$	= components of the torque acting on body i, through the joint connecting body i and body j, and expressed in the ith body frame
$C_i - x_i y_i z_i$	= Cartesian frame attached to the ith
g	= gravity acceleration
$\{f_{jk}\}, \{g_{jk}\}, \{h_{jk}\}$	= versors of the kth joint frame attached to the jth body
m_i	= mass of the ith body
$\{q\}$	= generalized coordinates
$\{q^{(i)}\}$	= generalized coordinates of the ith body
$[\Psi_q]$	= Jacobian matrix associated with constraint vector
dots $(\dot{})$	= differentiation w.r.t. time
$[\tilde{v}]$	= the skew-symmetric matrix obtained from vector $\{v\}$

The superscript on vectors (e.g. $\{a\}^{(i)}$) denotes the body frame in which is the components vector expressed (the subscript is omitted when i is the frame).
Square [ ] and curly { } brackets denote matrices and vectors, respectively.

1. Introduction

According to Huston [1], *multibody analyses have been applied more extensively with biodynamic modeling than with any other application area*. For example, crash-victim simulation is a widely studied research topic.

Although systematic multibody dynamics techniques are powerful tools for casting complex human models, there are few examples of linking between these and the experimental data provided by 3D video-based human motion analysis systems, e.g. [2].

Methods and technology used to capture the kinematics of human motion are well developed and commercially available. Their application into sport, rehabilitation, and clinical analysis is expanding and becoming a standard also among medical doctors. However, the authors of this paper believe that there is still a gap between the effective clinical use of the results given by theoretical 3D multibody dynamic models and the experimentally measured kinematic data. The type of dynamic analysis routinely performed in gait analysis is the interpretation of the experimental data obtained from the ground forces vectors measured by force plates. From such data, it is difficult to distinguish the torque components exerted at each joint.

The assessment of static force capability can also be performed by means of isokinetic tests. However, within the biomechanics scientific community, there is a debate about the reasons of the differences among peak torques, at lower limbs joints, measured with isokinetic tests and estimated through inverse dynamic analysis.

The main motivation for this study is the development of a technique for the experimental measurement of the driving torques of a human arm during voluntary movement.

The proposed technique is based on the use of an *ad hoc* inverse dynamics model where the kinematic data are experimentally collected by means of a human motion acquisition system.

The technique is currently being tested for the assessment of residual force capability of physically handicapped car drivers.

It is worth mentioning that this procedure also supplies the technicians with quantitative data about the workspace and speed of reach of the prospective handicapped driver.

To the best of the authors' knowledge, this is the first time that human motion analysis and inverse dynamic analysis have been applied in the field of car adaptation for handicapped drivers. The purpose is to provide the technician with quantitative data about the residual force capabilities and the kinetics of the driver's upper limbs. The availability of such data is the basis for an engineering approach to the design for the modification of a car's environment.

In this paper, the experimental setup, the dynamic model, and some numerical results for the case of an unrestrained voluntary movement of the upper limb will be described.

2. The Experimental Setup

The motion of the arm has been tracked by means of an APAS$^{\text{TM}}$ computerized optometry system for human motion analysis. The system used during this study was mainly composed of

- two portable analog video cameras (NTSC standard with capturing frequency of 60 Hz);
- a PC video card for grabbing the images recorded with the cameras;
- a calibration cube (each side one meter long);
- software for camera calibration, digitization and analysis of the markers position, velocity and acceleration.

The optometry system described is a common tool in biomechanics. The video camera image provides a 2D projection of the 3D space. The aim is to compute the spatial position of a marker from the knowledge of its position into the camera image space. The solution of the problem in 3D space requires at least two different projections. A well-known mapping procedure is the direct linear transformation (DLT) [4].

The experimental analysis procedure can be divided into three phases:

- video recording;
- digitization of the markers in each photogram;
- application of DLT mapping, smoothing and numerical differentiation of the Cartesian absolute position vector components of each marker.

The last two phases are executed by means of integrated software. In this study, raw data have been smoothed by means of cubic-splines. Moreover, frequency components higher than 15 Hz have been truncated.

Markers can be classified as static or dynamic. The positions of static markers are measured only once and are used for computing the initial position of joint Cartesian systems. The positions of dynamic markers are tracked in each photogram. Since our model is composed of three rigid bodies, nine dynamic markers (three for each human segment analyzed) were tracked. The chosen location of dynamic markers (dark points) and static markers (gray points) on the human arm analysed is shown in Figure 1.

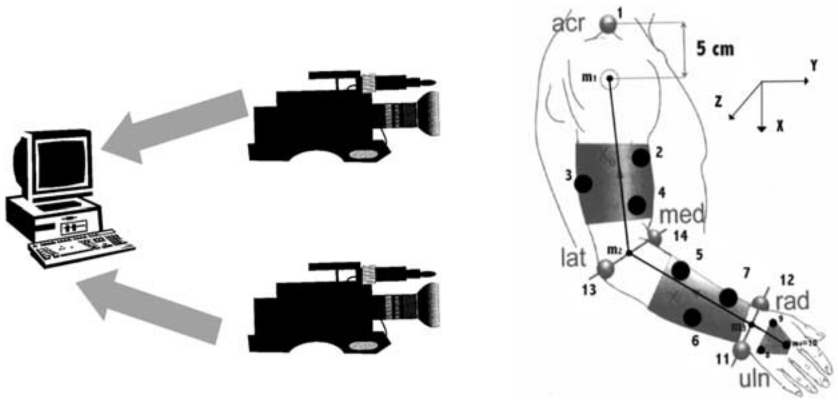

Figure 1. Position of static and dynamic markers on the arm.

3. Computerized Analysis of Data

The dynamic model has been developed under the hypothesis of rigid body motion. Because of measurement and calibration errors, skin movements, etc., the relative distance among markers on the same human segment will be not constant. Thus, the computation of the transformation matrices $[A_i]$ ($i = 1, 2, 3$), from the markers coordinates, follows the algorithm described in [11]. Similarly, the angular velocities and angular accelerations of each body segment have been computed from the velocities and accelerations of the markers by means of the method proposed by Sommer [12].

Alternatively, other algorithms may be chosen for computing the transform matrices [16, 19–24] and the kinematic characteristics of infinitesimal motion [17, 18, 21].

Pennestrì [6] reports a comparison of the numerical accuracy attained with various algorithms for computing Euler parameters from imprecise markers coordinates.

4. The Kinematic Model

The multibody methodology for the deduction of the kinematic and dynamics equations is the one outlined in [5]. The main reasons for the choice are the following:

- Possibility to define new kinematic pairs.
- Complete and exhaustive description both in textbooks and scientific papers.
- Availability of developed symbolic software tools specifically tailored for this methodology [7].

The human arm has been modeled by means of three rigid body segments: arm, forearm and hand. The shoulder is considered fixed (Figure 2). The first body (the

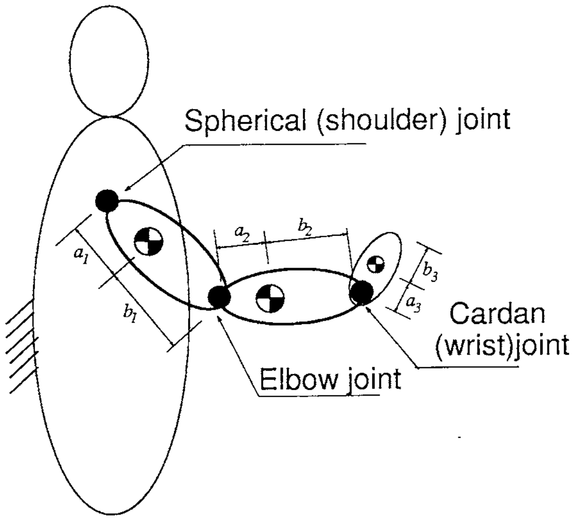

Figure 2. Topology of the 3D model of the human arm.

arm) is connected to the frame (upper torso) through a spherical joint. Arm and forearm are joined through a kinematic pair composed of two revolute pairs whose intersecting axes form a valgus angle $\alpha \approx 95$ deg. The relative motions of the forearm w.r.t. the arm are flexion-extension and pronation-supination.

The described movement is not reproduced by any of the joints available in [5]. Thus, a new joint has been created called an *elbow joint* with the above mentioned features.

The considered relative movements of the hand w.r.t. the forearm are yaw and pitch. Thus, the kinematic pair joining hand and forearm is composed of two revolute pairs with intersecting axes forming an angle of 90 deg (i.e. a cardan joint). The model has seven degrees of freedom.

The scalar constraints due to spherical and cardan joints can be found in textbooks, e.g. [5], and will be not repeated here. In the next section the scalar equations for the description of the elbow joint will be reported.

4.1. The Elbow Joint

For the purpose of modeling the kinematic pair connecting arm and forearm, a new joint (elbow joint) has been created. In particular, such a joint has two degrees of freedom. With reference to Figure 3, the first degree of freedom allows a rotation (flexion-extension) about the humeral transverse axis, whereas the second is a rotation (pronation-supination) about the axis of the forearm.

The equations of constraints that characterise an elbow joint are that:

- P_{12} and P_{22} coincide,
- versors $\{g_{12}\}$ and $\{f_{22}\}$ form an oriented angle α.

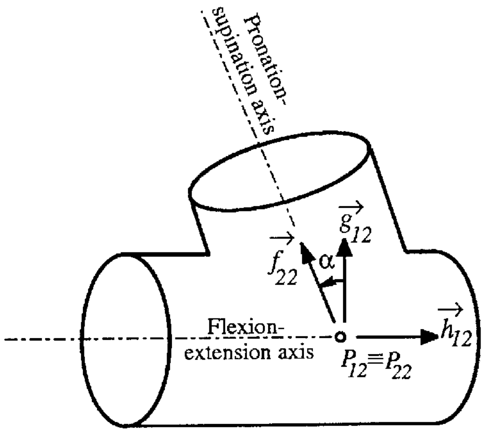

Figure 3. Elbow joint definition.

Table I. Degree-of-constraint of the joints.

Joint	No. of constraints
Spherical	3
Elbow	4
Cardan	4

These conditions are, respectively, specified by the basic spherical constraint

$$\{\Psi^s(P_{12}, P_{22})\} = \{0\} \tag{1}$$

and by the equation

$$\Psi^a \equiv (r_x - g_{12_x})^2 + (r_y - g_{12_y})^2 + (r_z - g_{12_z})^2 = 0, \tag{2}$$

where

$$\{u\} = [\tilde{f}_{22}]\{g_{12}\}, \tag{3}$$

$$\{r\} = ([I]\cos\alpha + (1 - \cos\alpha)\{u\}\{u\}^T + \sin\alpha[\tilde{u}])\{f_{22}\}. \tag{4}$$

4.2. Constraint Equations

The number of scalar constraints due to each kinematic pair is shown in Table I. Thus, taking into account the three normalization constraints for the three sets of Euler parameters, we can conclude that the vector of position constraints $\{\Psi\}$ has 14 components.

5. Dynamic Model of the Human Arm

It is assumed that the inertia properties of the hand segment are not influenced by the motion of the fingers.

5.1. Mass matrix

The mass matrix $[M]$ is

$$[M] = \begin{bmatrix} M_i & 0 & 0 \\ 0 & M_i & 0 \\ 0 & 0 & M_i \end{bmatrix}, \tag{5}$$

where [5]

$$[M_i] = \begin{bmatrix} \begin{bmatrix} m_i & 0 & 0 \\ 0 & m_i & 0 \\ 0 & 0 & m_i \end{bmatrix} & [0_{3\times 4}] \\ [0_{4\times 3}] & [4[G_i]^T[J^{(i)}][G_i]] \end{bmatrix}. \tag{6}$$

5.2. Generalized forces

The external forces considered are due to the weight $\{F_w\}$, to the quadratic velocity terms $\{F_c\}$ (centrifugal forces), and to joint torques $\{R\}$. The torques due to damping at the joints have been ignored [8]. However, if a reliable model is available, these can be also taken into account in our approach. In the following subsections the analytical expression of the generalized forces will be expressed.

5.2.1. *Centrifugal Forces*

The generalized centrifugal force acting on the ith mass is given by

$$\{F_{c_i}\} = \left\{ \begin{matrix} 0_{3\times 1} \\ 8[\dot{G}_i]^T[J^{(i)}][\dot{G}_i]\{e_i\} \end{matrix} \right\}. \tag{7}$$

The expression of $\dot{G}_i$ is not provided in [5]. However, it can be demonstrated [6] (see also Appendix) that

$$[\dot{G}_i] = \frac{1}{2}\big([G_i][\tilde{\omega}^{(i)}] - \{e_i\}\{\omega^{(i)}\}^T\big). \tag{8}$$

Thus, the vector of all generalized centrifugal forces is

$$\{F_c\} = \left\{ \begin{matrix} F_{c_1} \\ F_{c_2} \\ F_{c_3} \end{matrix} \right\}. \tag{9}$$

5.2.2. *Weight Forces*

The generalized weight force acting on the ith mass is given by

$$\{F_{w_i}\} = \left\{ \begin{array}{c} m_i g \\ 0_{6\times 1} \end{array} \right\}. \tag{10}$$

Thus, the vector of all generalized weight forces is

$$\{F_w\} = \left\{ \begin{array}{c} F_{w_1} \\ F_{w_2} \\ F_{w_3} \end{array} \right\}. \tag{11}$$

5.2.3. *Joint Torques*

The generalized forces on body i can be computed by means of the following expression [5]

$$\{R_j\} = \left\{ \begin{array}{c} \{0_{3\times 1}\} \\ 2[E_i]^T\{T\} \end{array} \right\}, \tag{12}$$

when the components of applied torque $\{T\}$ are given in the inertial frame, or

$$\{R_j\} = \left\{ \begin{array}{c} 0_{3\times 1} \\ 2[G_i]^T\{T\}^{(i)} \end{array} \right\}, \tag{13}$$

when the same components are expressed in the ith body reference frame.

- *Generalized forces due to the motor torque* $\{T_{10}\}^1 = \{T_{10x_1}\ T_{10y_1}\ T_{10z_1}\}$ *exerted on the upper-arm (body 1) through the spherical joint.*

$$\{R1\} = T_{10x_1} \left\{ \begin{array}{c} 0_{3\times 1} \\ 2[G_1]^T\{f_{11}\}^{(1)} \end{array} \right\}, \tag{14}$$

$$\{R2\} = T_{10y_1} \left\{ \begin{array}{c} 0_{3\times 1} \\ 2[G_1]^T\{g_{11}\}^{(1)} \end{array} \right\}, \tag{15}$$

$$\{R3\} = T_{10z_1} \left\{ \begin{array}{c} 0_{3\times 1} \\ 2[G_1]^T\{h_{11}\}^{(1)} \end{array} \right\}. \tag{16}$$

- *Generalized forces due to the motor torque exerted on the upper arm (body 1) through the elbow joint.*

$$\{R4\} = T_{12y_1} \left\{ \begin{array}{c} 0_{3\times 1} \\ 2[G_1]^T\{g_{12}\}^{(1)} \end{array} \right\}, \tag{17}$$

$$\{R7\} = -T_{21x_2} \left\{ \begin{array}{c} 0_{3\times 1} \\ 2[G_1]^T[A_1]^T[A_2]\{f_{22}\}^{(2)} \end{array} \right\}. \tag{18}$$

- *Generalized forces due to the motor torque exerted on the arm (body 2) through the elbow joint.*

$$\{R5\} = -T_{12y_1}\left\{\begin{array}{c} 0_{3\times 1} \\ 2[G_2]^T[A_2]^T[A_1]\{g_{12}\}^{(1)} \end{array}\right\}, \tag{19}$$

$$\{R6\} = T_{21x_2}\left\{\begin{array}{c} 0_{3\times 1} \\ 2[G_2]^T\{f_{22}\}^{(2)} \end{array}\right\}. \tag{20}$$

- *Generalized forces due to the motor torque exerted on the arm (body 2) through the wrist joint.*

$$\{R8\} = T_{32y_2}\left\{\begin{array}{c} 0_{3\times 1} \\ 2[G_2]^T\{g_{23}\}^{(2)} \end{array}\right\}, \tag{21}$$

$$\{R10\} = T_{32z_2}\left\{\begin{array}{c} 0_{3\times 1} \\ 2[G_2]^T\{h_{23}\}^{(2)} \end{array}\right\}. \tag{22}$$

- *Generalized forces due to the motor torque exerted on the hand (body 3) through the wrist joint.*

$$\{R9\} = -T_{32y_2}\left\{\begin{array}{c} 0_{3\times 1} \\ 2[G_3]^T[A_3]^T[A_2]\{g_{23}\}^{(2)} \end{array}\right\}, \tag{23}$$

$$\{R11\} = -T_{32z_2}\left\{\begin{array}{c} 0_{3\times 1} \\ 2[G_3]^T[A_3]^T[A_2]\{h_{23}\}^{(2)} \end{array}\right\}. \tag{24}$$

Thus, a vector $\{R\}$ can be defined as

$$\{R\} = [\mathcal{R}]_{21\times 7}\{\mathcal{T}\}, \tag{25}$$

where

$$[\mathcal{R}]_{21\times 7} = \begin{bmatrix} R1 & R2 & R3 & R4 & -R7 & 0 & 0 \\ 0 & 0 & 0 & -R5 & R6 & R8 & R10 \\ 0 & 0 & 0 & 0 & 0 & -R9 & -R11 \end{bmatrix} \tag{26}$$

is a block matrix and

$$\{\mathcal{T}\} = \left\{\begin{array}{c} T_{10x_1} \\ T_{10y_1} \\ T_{10z_1} \\ T_{12y_1} \\ T_{21x_2} \\ T_{32y_3} \\ T_{32z_3} \end{array}\right\} \tag{27}$$

is the vector of unknown torque components.

5.3. DYNAMIC EQUATIONS

For our model, $[M]$ will be a square matrix 21×21, $[\Psi_q]$ is a rectangular matrix 14×21. For a free movement of the arm, it is convenient to split the vector $\{Q\}$ of generalized forces into three parts:

$$\{Q\} = \{R\} + \{F_w\} + \{F_c\}. \tag{28}$$

The first vector $\{R\}$ depends on the unknown torque components at the joints, whereas $\{F_w\}$ contains the generalized forces due to the weight.

Thus, separating the unknowns (i.e. torque components and internal constraint forces) from the known forces (i.e. inertia, centrifugal and weight forces), one has:

$$\{R\} - [\Psi_q]^T\{\lambda\} = [M]\{\ddot{q}\} - \{F_w\} - \{F_c\}. \tag{29}$$

Finally, Equation (29) can be rewritten in the form

$$[\mathcal{R} \;\; \Psi_q^T]_{21\times 21} \left\{ \begin{array}{c} \{\mathcal{T}\} \\ \{-\lambda\} \end{array} \right\} = [M]\{\ddot{q}\} - \{F_w\} - \{F_c\}, \tag{30}$$

which can be readily solved w.r.t. $\{\mathcal{T}\}$ (Torque components) and $\{\lambda\}$ (Lagrange's multipliers), once the inertia properties are known and the kinematics experimentally measured. If needed, the constraint forces can be computed from the Lagrange multipliers.

6. Numerical Example

The model has been applied to unrestrained voluntary movement of an arm of a healthy male subject.

1. *Camera calibration*
   The calibration phase is executed by the APAS software. In particular, two views (one for each camera) of the calibration cube are used. The absolute reference frame is generated, as shown in Figure 5, from the position of the markers on the calibration cube.
2. *Static measurements*
   The purpose of this phase is the collection of data necessary for anthropometric analysis and for the location of body reference frame. More details are given in [10].
   The arrangement of the markers (both static and dynamic), similar to those suggested by Schmidt et al. [9], is depicted in Figure 1.

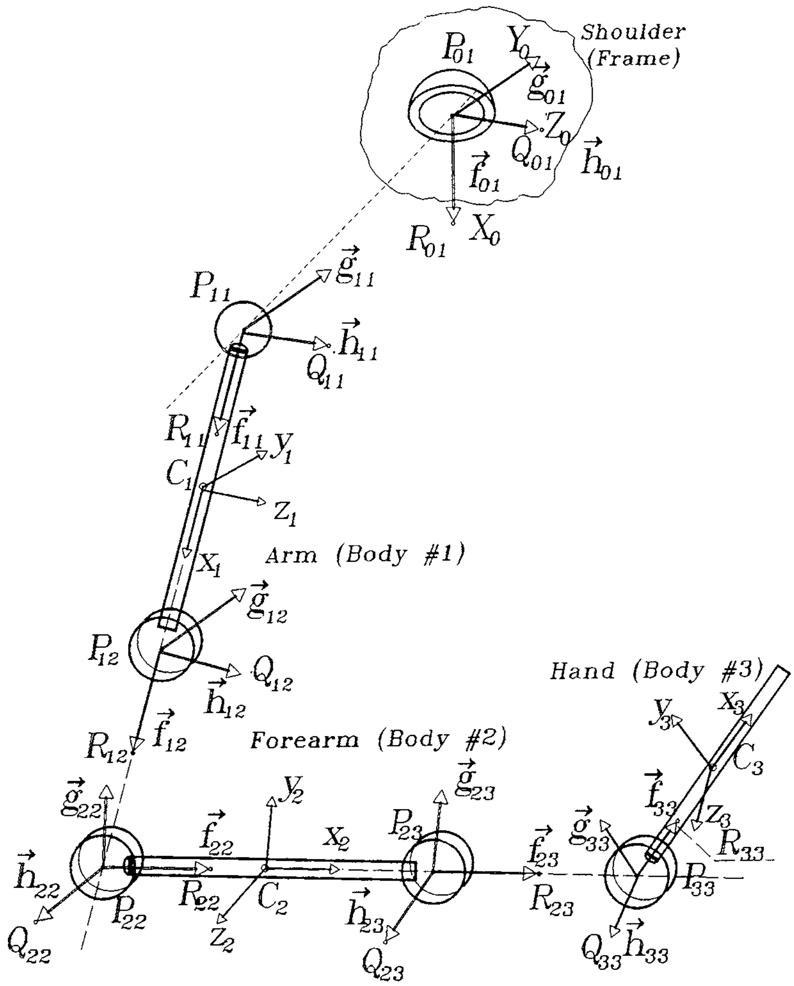

Figure 4. Joint and body Cartesian systems.

3. *Anthropometric data*
   The main anthropometric data have been obtained by means of the static measurements on a male subject weighting 65 kg and 1.74 m tall. The collected data have been substituted into a formula reported in [13, 14]. With reference to the nomenclature of Figure 1, the estimated geometrical and inertial data are summarized in Table II.
4. *Kinematic measurements*
   After removing the static markers, the dynamic markers are tracked for the kinematic analysis of the arm under free movement.
   In particular, as shown in Figure 6, the tracked movement is the lifting and lowering of the arm. The subject had been requested to make a planar movement parallel to the sagittal plane.

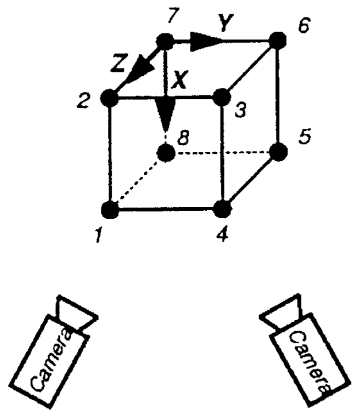

Figure 5. Calibration cube and inertial Cartesian frame.

Table II. Anthropometric data (computed according to [13, 14]).

Body i	a_i (m)	b_i (m)	m_i (kg)	$J_{xx}^{(i)}$ ($kg \cdot m^2$)	$J_{yy}^{(i)}$ ($kg \cdot m^2$)	$J_{zz}^{(i)}$ ($kg \cdot m^2$)
1 (arm)	0.118	0.151	1.85	$0.42 \cdot 10^{-2}$	$1.40 \cdot 10^{-2}$	$1.40 \cdot 10^{-2}$
2 (forearm)	0.114	0.151	1.05	$2.05 \cdot 10^{-3}$	$6.85 \cdot 10^{-3}$	$6.85 \cdot 10^{-3}$
3 (hand)	0.039	0.038	0.39	$1.28 \cdot 10^{-4}$	$2.13 \cdot 10^{-4}$	$2.13 \cdot 10^{-4}$

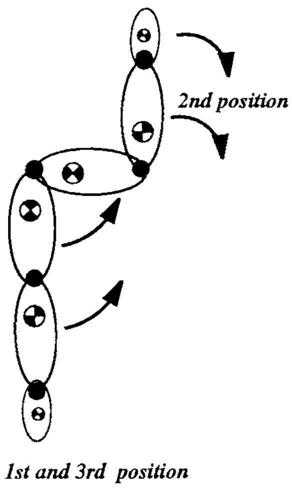

Figure 6. Scheme of the tracked arm movement.

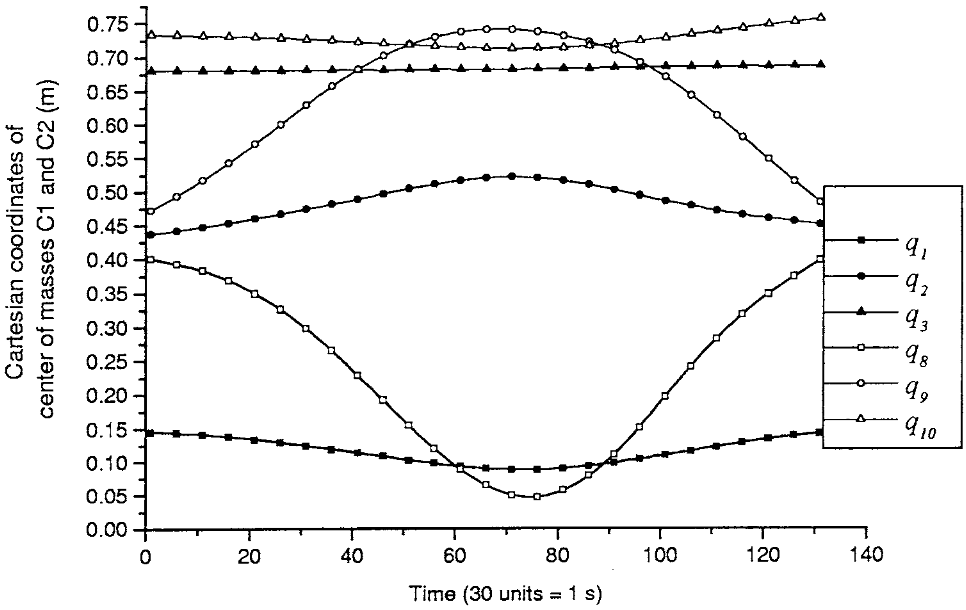

Figure 7. Center of masses cordinates.

Initially, all the segments are perpendicular to the ground in the rest position. In the middle configuration, the arm segment is parallel to the ground, whereas the forearm and the hand segments are perpendicular to it. The initial and final positions coincide.

After raw data smoothing and regularization [11, 12], the final values of generalized coordinates vs. time are plotted in Figures 7–10.

5. *Computation of torques*

No further refinement is applied to make the generalized coordinates fully consistent with the constraint equations. However, the difference of torque components computed with and without the generalized coordinates refinement is about 10%.

Thus, the generalized coordinates $\{q\}$ and their numerical derivatives, $\{\dot{q}\}$, $\{\ddot{q}\}$, were directly substituted into Equation (30) and subsequently solved w.r.t. $\{\mathcal{T}\}$. The estimated torque components vs. time are plotted in Figures 11 and 12.

7. Conclusions

The order of magnitude of the numerical results is consistent with those reported in the literature [2, 15]. However, the values of torque component $T_{21_{x2}}$ are an exception. They seem to have been too much influenced by the measurement errors of our experimental apparatus. Likely, a reduction of these errors can be achieved by increasing the number of cameras.

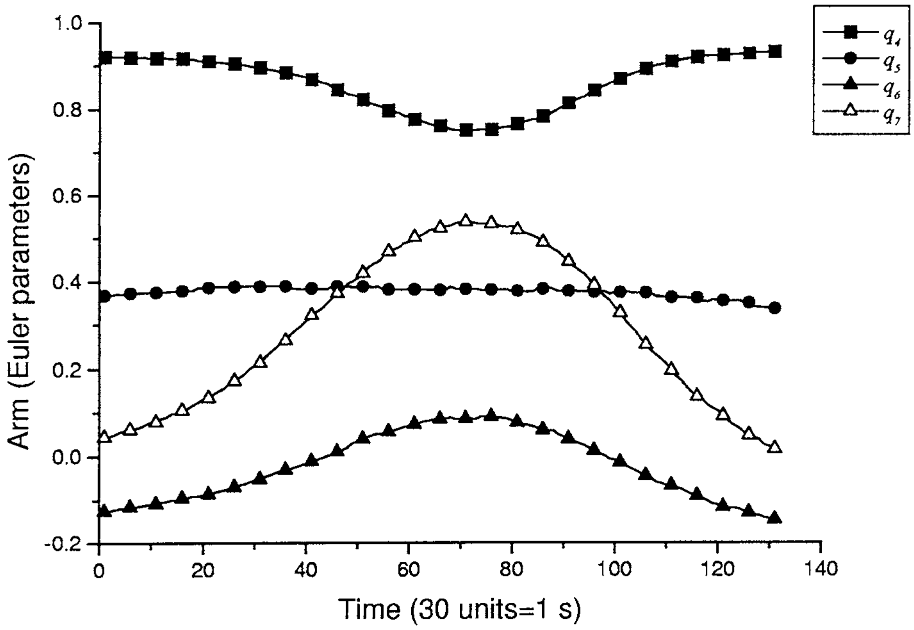

Figure 8. Euler parameters of the arm.

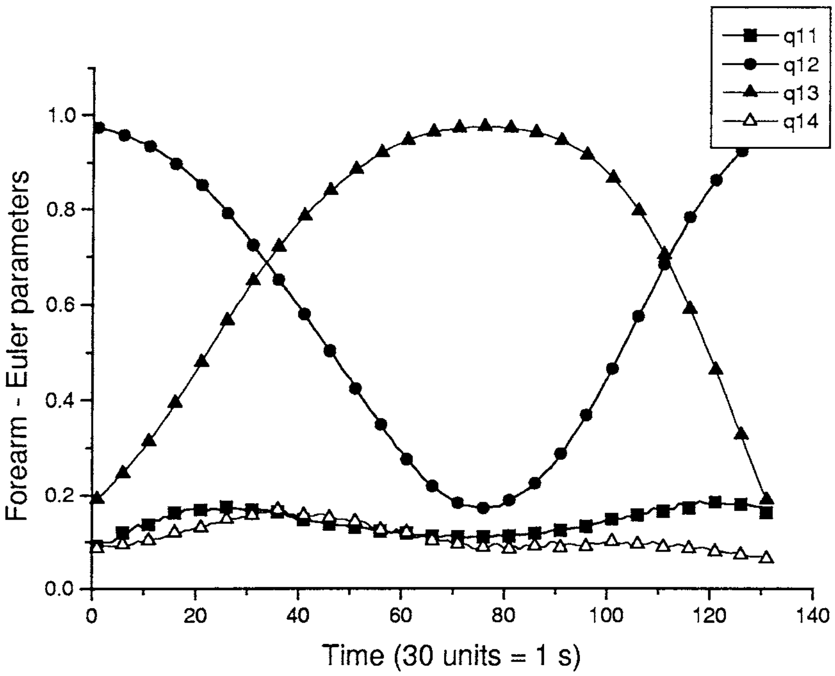

Figure 9. Euler parameters of the forearm.

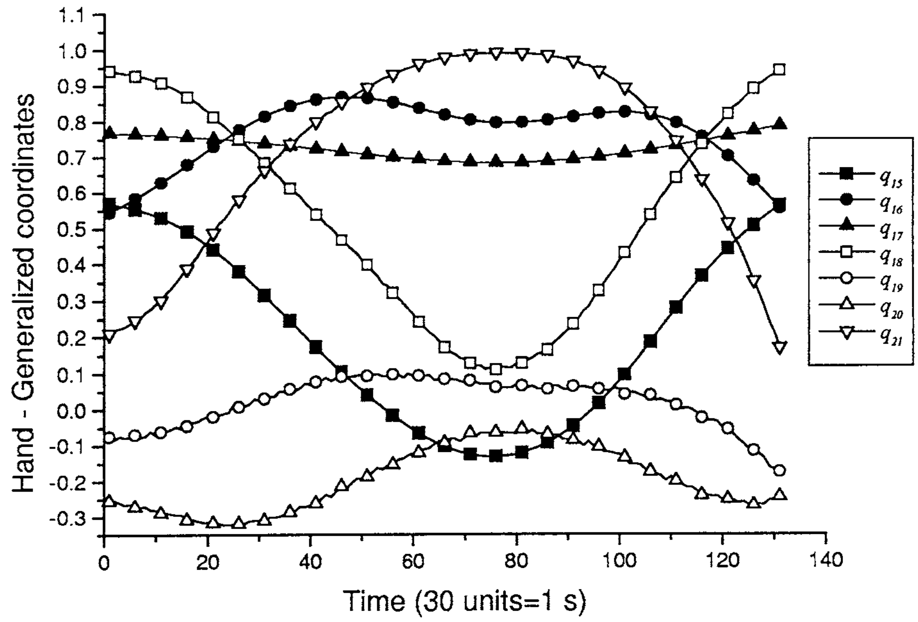

Figure 10. Generalized coordinates of the hand.

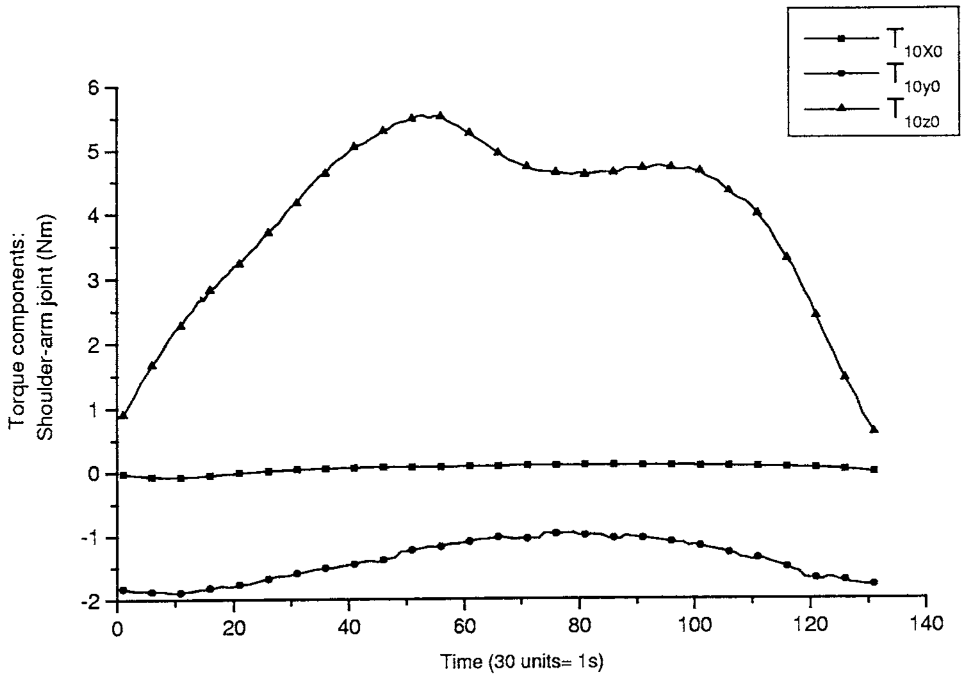

Figure 11. Torque components at the joint shoulder-arm.

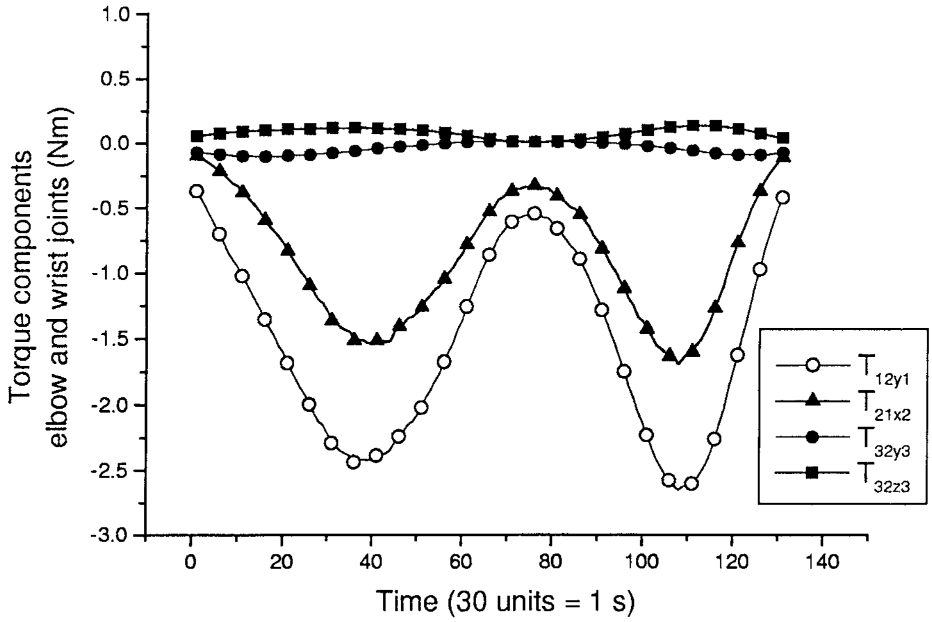

Figure 12. Torque components at the elbow and wrist joint.

The model herein described could be used as a tool for the classification of motion and residual force capabilities of physically handicapped people. This classification is especially useful in the field of the adaptation of the car environment to the needs of handicapped drivers. Currently, such a classification is based only on clinical observations. The idea pursued by this research is the classification based on a set of instrumented experimental analyses. The research team is also working on the dynamic modeling of other significant driver movements, such as steering. The procedure is being tested at the site of a company adapting the car environment for handicapped drivers. The results obtained give a rational basis for the choice and calibration of the auxiliary devices installed on the car.

Appendix

Matrix $[G_i]$ has the following property

$$[G_i]^T[G_i] = [I_4] - \{e_i\}\{e_i\}^T.$$

Taking into account that

$$\begin{aligned}[\tilde{\omega}^{(i)}] &= 2[G_i][E_i]^T[E_i][\dot{G}_i]^T \\ &= 2[G_i][\dot{G}_i]^T,\end{aligned}$$

follows

$$[G_i]^T[\tilde{\omega}^{(i)}] = 2[G_i]^T[G_i][\dot{G}_i]^T$$

$$
\begin{aligned}
&= 2[\dot{G}_i]^T - 2\{e_i\}\{e_i\}^T[\dot{G}_i]^T \\
&= 2[\dot{G}_i]^T - 2\{e_i\}\{\dot{e}_i\}^T[G_i]^T \\
&= 2[\dot{G}_i]^T + \{e_i\}\{\omega^{(i)}\}^T.
\end{aligned}
$$

Acknowledgements

The authors wish to express their gratitude for the financial and logistic support received from Guidosimplex s.n.c. and for technical discussions with its manager Mr. Stefano Venturini.

References

1. Huston, R.L., *Multibody Dynamics*, Butterworth-Heinemann, Portland, 1990, 366–370.
2. Terze, Z., Lefeber, D. and Muftić, D., 'Null space integration method for constrained multibody system with no constraint violation', in *Advances in Computational Multibody Dynamics*, J.A.C. Ambrósio and W. Schielen (eds), IDMEC/IST Lisbon, Portugal, September 20–23, 1999, 789–799.
3. Silva, M.P.T., Ambrósio, J.A.C. and Pereira, M.S., 'Biomechanical model with joint resistance for impact simulation', *Multibody System Dynamics* **1**, 1997, 65–84.
4. Wood, G.A. and Marshall, R.N., 'The accuracy of the DLT exrapolation in three-dimensional film-analysis', *Journal of Biomechanics* **19**, 1986, 781–785.
5. Haug, E.J., *Computer-Aided Kinematics and Dynamics of Mechanical Systems*, Vol. I, Allyn and Bacon, Boston, MA, 1989.
6. Pennestrì, E., *Elements of Technical and Computational Dynamics*, Editrice Aracne, Rome, 2000 [in Italian].
7. Brutti, C., Pennestrì, E. and Urbinati, F., 'Kinematic analysis of spatial mechanisms by means of Maple', *MapleTech* **5**, 1999, 49–57.
8. Latash, M.L., Arvin, A.S. and Zatsiorsky, V.M., 'The basis of a simple synergy: Reconstruction of joint equilibrium trajectories during unrestrained arm movements', *Human Movement Sciences* **18**, 1999, 3–30.
9. Schmidt, R., Disselhorst-Klug, C., Silny, J. and Rau, G., 'A measurement procedure for the quantitative analysis of the free upper-extremity movements', in *Proceedings Fifth International Symposium on the 3-D Analysis of Human Movement*, Chattanooga, TN, July 2–5, M. Whittle (ed.), 1998, 47–54.
10. Renzi, A., 'Telemetry surveying and 3D dynamic modeling of the human upper limb', Tesi di Laura, University of Rome 'Tor Vergata', A.A.1998-99 [in Italian].
11. Woltring, H.J., Huiskes, R., de Lange, A. and Veldpaus, F.E., 'Finite control and helical axis estimation from noisy landmark measurements in the study of human joint kinematics', *Journal of Biomechanics* **18**, 1985, 379–389.
12. Sommer, H.J., 'Determination of first and second order instant screw parameters from landmark trajectories', *ASME Journal of Mechanical Design* **114**, 1992, 274–282.
13. Clauser, C.E., Young, J.W. and McConville, J.T., 'Weight, volume and center of mass segments of the human body', Wright Patterson Air Force Base, AMRL-TR-69-70, 1969.
14. Chandler, R.F., Clauser, C.E. and McConville, J.T., 'Investigation of properties of the human body', Wright Patterson Air Force Base, AMRL-TR-74137, 1975.
15. Raikova, R., 'A general approach for modelling and mathematical investigation of the human upper limb', *Journal of Biomechanics* **25**, 1992, 857–867.

16. Angeles, J., 'Automatic computation of the screw parameters of rigid body motions. Part I: Finitely-separated positions', *ASME Journal of Dynamic Systems, Measurement and Control* **108**, 1986, 32–38.
17. Angeles, J., 'Automatic computation of the screw parameters of rigid body motions. Part II: Infinitesimally separated positions', *ASME Journal of Dynamic Systems, Measurement and Control* **108**, 1986, 39–43.
18. Angeles, J., 'Computation of rigid-body angular acceleration from point-acceleration measurements, *ASME Journal of Dynamic Systems, Measurement and Control* **109**, 1987, 124–127.
19. Gupta, K.C. and Chutakanonta, P., 'Accurate determination of object position from imprecise data', *ASME Journal of Mechanical Design* **120**, 1998, 559–564.
20. Gupta, K.C., 'Measures of positional error for a rigid body', *ASME Journal of Mechanical Design* **119**, 1997, 346–348.
21. Laub, A.J. and Shifflett, G.R., 'Linear algebra approach to the analysis of rigid body displacement from initial and final position data', *ASME Journal of Applied Mechanics* **49**, 1982, 213–216.
22. Shifflett, G.R. and Laub, A.J., 'The analysis of rigid body motion from measured data', *ASME Journal of Dynamic Systems, Measurement and Control* **117**, 1995, 578–584.
23. Spoor, C.W. and Veldpaus, F.E., 'Rigid body motion calculated from spatial coordinates of markers', *Journal of Biomechanics* **134**, 1980, 391–393.
24. Veldpaus, F.E., Woltring, H.J. and Dortmans, L.J.M.G., 'Least squares algorithm for the equiform transformation from spatial marker coordinates', *Journal of Biomechanics* **21**(1), 1988, 45–54.